Activation of skeletal muscle-resident glial cells upon nerve injury

Daisy Proietti, Lorenzo Giordani, Marco de Bardi, Chiara d'Ercole, Biliana Lozanoska-Ochser, Susanna Amadio, Cinzia Volontè, Sara Marinelli, Antoine Muchir, Marina Bouchè, et al.

JCI insight

Activation of skeletal muscle-resident glial cells upon nerve injury

Daisy Proietti, … , Pier Lorenzo Puri, Luca Madaro

JCI Insight. 2021. https://doi.org/10.1172/jci.insight.143469.

Research In-Press Preview Muscle biology

Graphical abstract

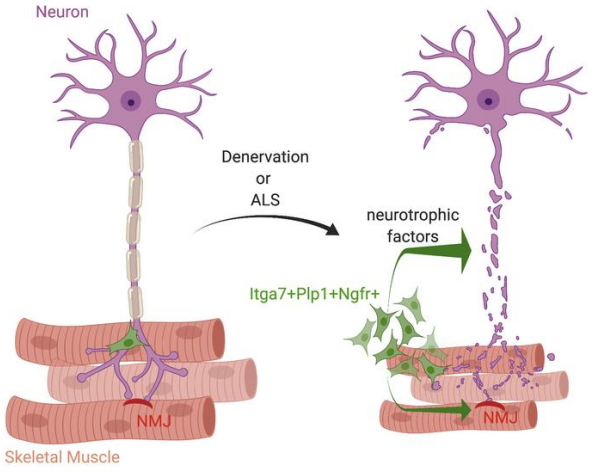

TITLE PAGE

Title

Activation of skeletal muscle-resident glial cells upon nerve injury

Authors

Daisy Proietti[1,2], Lorenzo Giordani[3], Marco De Bardi[1], Chiara D'Ercole[2], Biliana Lozanoska-Ochser[2], Susanna Amadio[1], Cinzia Volontè[1-4], Sara Marinelli[5], Antoine Muchir[3], Marina Bouchè[2], Giovanna Borsellino[1], Alessandra Sacco[6], Pier Lorenzo Puri[6] and Luca Madaro[1,2,7]*

Affiliations

[1] IRCCS Fondazione Santa Lucia (FSL); Rome; Italy

[2] Dept AHFMO, University of Rome "la Sapienza", Via A. Scarpa 14, 00161 Rome, Italy

[3] Sorbonne Université, INSERM UMRS 974, Association Institut de Myologie, Centre de Recherche en Myologie, 75013 Paris, France.

[4] CNR, Institute for Systems Analysis and Computer Science, Via Dei Taurini 19, 00185 Rome

[5] CNR - National Research Council, Institute of Biochemistry and Cell Biology, 00015 Monterotondo Scalo (RM), Italy.

[6] Development, Aging and Regeneration Program, Sanford Burnham Prebys Medical Discovery Institute, La Jolla, CA, USA

[7] Lead Contact

*Correspondence: Luca Madaro, via Antonio scarpa 14/16 00143 Rome (Italy), +39 0649766573 luca.madaro@uniroma1.it

Conflict of interest statement

The authors have declared that no conflict of interest exists.

ABSTRACT

Here, we report on the identification of Itga7-expressing muscle resident glial cells activated by loss of NMJ integrity. Gene expression analysis at bulk and single cell level revealed that these cells are distinct from Itga7-expressing muscle satellite cells. We show that a selective activation and expansion of Itga7-positive glial cells occurs in response to muscle nerve lesion. Upon activation, muscle glial-derived progenies expressed neurotrophic genes, including Ngfr, which enables their isolation by FACS. We show that activated muscle glial cells also expressed genes potentially implicated in ECM remodeling at NMJs. Among them, we observed Tenascin C (Tnc), which was highly expressed by muscle glial cells activated upon nerve injury, and preferentially localized to NMJ. Interestingly, we observed that while the activation of muscle glial cells by acute nerve injury was reversible, upon NMJ repair. By contrast, in a mouse model of Amyotrophic Lateral Sclerosis (ALS), in which NMJ degeneration is progressive, muscle glial cells steadily increased over the course of the disease; however, they exhibited an impaired neurotrophic activity, suggesting that pathogenic activation of glial cells may be implicated in ALS progression.

INTRODUCTION

Skeletal muscle homeostasis is maintained by a large network of muscle-resident cells, that coordinate the response to homeostatic perturbations, such as muscle or nerve injury (1, 2).

Among these cells, muscle satellite cells (MuSCs) are the bonafide muscle stem cells that exist in a quiescent state during homeostasis in adult tissues and become activated in response to acute muscle damage or in chronic degenerative conditions (3–8). In addition to their absolute requirement for regeneration of injured muscle, recent studies have reported that MuSCs may also participate in the maintenance of neuro-muscular junction (NMJ) integrity and regeneration upon nerve injury (9, 10). Nerve injury and repair are events closely associated with the process of muscle regeneration; however, the precise contribution of MuSCs to NMJ regeneration is poorly understood. Likewise, whether additional muscle-resident cell types contribute to neurite growth and extension toward regenerating fibers to restore functional NMJs remains unknown.

We and others have recently reported on the activation of muscle-resident mesenchymal progenitors – the fibro adipogenic progenitors (FAPs), and their expansion following denervation (11). In addition to FAPs, resident macrophages have also been implicated in the process of NMJ repair following denervation or injury (9, 10, 12, 13). Interestingly, alterations in function and number of MuSCs and FAPs have been observed in neuromuscular disorders, such as Amyotrophic Lateral Sclerosis (ALS), in which loss of NMJ integrity occurs progressively (14, 15)

In postnatal life, the disruption of skeletal muscle-nerve cross talk leads to muscle atrophy and fibrosis (16–18), eventually leading to irreversible paralysis in conditions of complete nerve loss (i.e. traumatic spinal cord injury) or progressive loss of NMJ (e.g. chronic neuromuscular disorders) (19). Therefore, identification of the cell types activated by nerve injury and an improved understanding of their functional interactions is imperative in order to develop novel therapeutic strategies to counter the effect of muscle denervation.

In this study, we performed gene expression analysis in both bulk and single cells isolated from limb muscle following nerve injury with the aim to identify the cellular players that might contribute to nerve repair.

RESULTS

Nerve injury activates a neurotrophic program in Itga7+ non-satellite cells

The contribution of Itga7-expressing MuSCs to the maintenance of NMJ integrity, and regeneration upon nerve injury was previously reported by Liu et al 2015 and Liu et al. 2017 (9, 10). These studies prompted our interest in the transcriptional profiles of Itga7+ cells isolated from limb muscles of mice either unperturbed or exposed to nerve injury. To this end, we performed RNAseq analysis on Itga7+/Sca1-/Ln- cells (from now on, referred to as Itga7+ cells) isolated by FACS from limb muscles of 3-month-old mice, at 3 days after denervation by sciatic nerve severing, and compared to Itga7+ cells isolated from control mice. Heatmap comparison revealed extensive alterations of the transcriptional profile in Itga7+ cells isolated post-nerve injury, compared to unperturbed controls, with a clear bias toward up-regulation of genes which accounted for the vast majority of the differentially expressed genes (Figure 1a). Notably, most of the upregulated genes were those associated with neuronal growth and repair pathways, including Nerve Growth Factor Receptor (Ngfr), Sonic Hedgehog (Shh) Tenascin-C (Tnc), Neuronal Cell Adhesion Molecule (NRCAM), Glial Cell Derived Neurotrophic Factor (Gdnf), and the glial lineage-specific transcription factors Oligodendrocyte lineage genes (Olig1) (Figure 1a). Other genes of alternative mesenchymal lineages, but recently implicated in neurogenesis (e.g. Runx2) (20) were also found upregulated in Itga7+ cells isolated following nerve injury. Moreover, gene ontology analyses of RNAseq data predicted the activation of “nervous system development” and “axon guidance” among the main activated pathways (Figure 1b).

The upregulation of neurotrophic genes in Itga7+ cells after denervation suggests that this population includes cell types endowed with potential nerve repair activities. Thus, in order to identify this population, we sought to determine whether the activation of the neurotrophic gene program also occurred in Itga7+ cells isolated from muscles subjected to sciatic nerve crush - a reversible lesion that is typically followed by repair and restoration of NMJ integrity (21). Indeed, the upregulation of neurotrophic genes was also detected by qPCR analysis in Itga7+ cells following sciatic nerve crush (Figure 1c). Interestingly, activation of the same genes was also observed in cells

isolated using the Satellite Cells isolation kit (Miltenyi Biotec) magnetic strategy that is based on lineage marker exclusion of Itga7-negative muscle-resident cells (Suppl. Figure 1a).

Given the recent studies showing that Itga7-expressing cell populations in muscle include cellular subsets divergent in developmental origin from the actual MuSCs (22), we utilized the PAX7^{CreER};tdTomato$^{f/f}$ mouse model, which allows MuSCs lineage tracing (23), in order to unequivocally determine whether the activation of the neurotrophic gene program occurs in MuSCs or the non-MuSC cell fraction among the Itga7+ cells. In this mouse model, tamoxifen treatment leads to the permanent expression of tomato fluorescent protein in Pax7+ MuSCs (Suppl. Figure 1b). Seven days after tamoxifen treatment, 3-month-old mice were subjected to nerve injury and analyzed 3 days later (Figure 1d). As expected, Itga7+Tomato+ cells isolated from limb muscles of uninjured mice or following sciatic nerve crush expressed high level of the MuSC-identity genes Pax7 and Vcam1, whereas the Itga7+Tomato- cell population did not express these markers (Figure1e). However, upon denervation, only the Itga7+Tomato- fraction expressed Ngfr, Shh, Tnc, Nrcam and Gdnf, indicating the induction of a neurotrophic signalling pathway in the Pax7-negative fraction of Itga7+ cells (Figure 1e, Suppl. Figure 1c). These observations also indicate that among the cells isolated with the Satellite Cells isolation kit (Miltenyi Biotec), non-myogenic Itga7+ and Pax7 negative cell types might also co-segregate with the myogenic fraction.

Overall, these findings show transcriptional activation of a neurotrophic program in the non-myogenic fraction of Itga7+ cells and suggest their potential involvement in the functional cross-talk between muscle resident cells and NMJ in response to nerve injury.

scRNA-seq reveals heterogeneity within the Itga7+ muscle resident cells

Recently, the heterogeneous composition of muscle resident mononuclear cells has been dissected using high resolution cartography by scRNA-seq. This strategy has revealed the identity of a new MuSCs-independent myogenic population among the Itga7+ cells, referred to as Smooth Muscle Mesenchymal Cells (SMMCs) (22). To further determine whether the activation of the neurotrophic program upon nerve injury occurred in SMMC or in other sub-populations within Itga7+ cells, we performed single-cell RNA-seq (scRNA-seq) transcriptome profiling in Itga7+ cells isolated

from limb muscles of mice 3 days following sciatic nerve crush or control mice. By using the 10x Genomics' single-cell RNA-seq (scRNA-seq) technology we obtained a total of 3949 cells analyzed. Clustering analysis identified 11 different groups (Suppl. Figure 2a). Based on markers expression we could clearly identify three major populations that were composed of multiple sub-clusters (Figure 2a-b). In particular, we detected MuSCs, as Pax7+, Myf5+ and Vcam1+ expressing cells, smooth muscle mesenchymal cells (SMMCs), as Myh11+ expressing cells and glial cells as Plp1 and Mpz expressing cells (Figure 2a).

Interestingly, within the SMMCs cell population we could distinguish a Myl9+Rgs5^{low} and Myl9+Rgs5^{high} subpopulations (Suppl. Figure 2b). In line with this observation, Rgs5, Myl9 and Plp1 expression was evident in the tomato-negative fraction of tamoxifen treated PAX7.Cre_tdTomato mice (Suppl. Figure 2c). The gene expression profile of the smaller clusters (less than 150 cells) was indicative of myotendinous (Scx^{high} expressing cells), endothelial (Pecam1^{high}) and mesenchymal (as Ly6a/Ly6e^{pos} and Pdgfra^{pos}) lineages (Figure 2b). However, it is likely that the presence of these clusters is due to contamination from Itga7$^{low/neg}$ populations.

Plp1+ glial cells are the major Itga7+ population responsive to denervation.

We focused our analysis on the three major cell types identified by scRNAseq analysis among the Itga7+ cells isolated following nerve injury – i.e. MuSCs, SMMCs and glial cells. We observed a similar distribution of MuSCs and SMMCs in both healthy and denervated muscle (Figure 3a). By contrast, we observed a specific increase in Plp1+ cells in response to nerve injury. To validate this finding, we denervated mice by nerve crush injury, and at 12h before harvest we administered an intraperitoneal injection of EdU. EdU incorporation analysis revealed a significant proportion of proliferating Plp1+ cells at 3 days following sciatic nerve crush (Suppl. Figure 3a). The gene expression profile of nerve injury-activated Plp1+ cells largely overlapped with those of glial cells recently described by both De Micheli et al. and Giordani et al. (22, 24) (Suppl. Figure 3b); however, there was no significant overlap with other populations (in particular with MuSCs and SMMCs) (Suppl. Figure 3b). In addition, these cells were enriched in additional markers known to be expressed by glial/Schwann cells (Suppl. Figure 3c).

158 Furthermore, we noted extensive alterations in gene expression in Plp1+ cells following nerve
159 injury, compared to control muscle, while only a few genes were significantly altered in MuSCs and
160 SMMCs (Suppl. Figure 3d). Single cell RNAseq analysis revealed that Plp1+ glial cells are
161 characterized by a neurotrophic signature (Figure 3b-c and Suppl. Figure 3d), with most of the
162 upregulated genes coinciding with those identified in the bulk Itga7+ cells shown in Figure 1 – i.e.
163 Ngfr, Tnc, Gdnf, Runx2 and other genes strictly related to nerve development (Figure 3b-c). Among
164 these genes, the Ngfr was used to identify these cells, since it was found to be specifically expressed
165 in glial-cells, and no other muscle resident cells, in response to nerve injury, by an independent
166 scRNAseq analysis post-denervation (25). It is interesting to note that Hicks et al. have previously
167 shown that Ngfr is transiently expressed in human MuSC progenitors during the generation of hiPSC-
168 derived MuSCs (26). Our data indicate that Ngfr expression discriminates glial cells from MuSCs
169 within a common pool of Itga7+ cells. Indeed, Ngfr+ cells were only detected among the Itga7+
170 population in the muscle at 3 days after denervation, while only a negligible number of Ngfr+ cells
171 were present in control muscle (Figure 3d-e, Suppl. Figure 4a-c). There were no significant changes
172 in the number of Ngfr-Itga7+ cells after nerve injury (Suppl. Figure 4d), thus confirming that the main
173 cell type responding to denervation are the muscle- resident glial cells. Indeed, the number of Pax7+
174 cells did not change at 3 days after nerve injury and Pax7 did not co-localize with Ngfr in serial
175 muscle sections (Suppl. Figure 4e-f). Moreover, the induction of neurotrophic genes, including Ngfr,
176 but also Plp1, Tnc, Nrcam and Gdnf, was only detected in Ngfr+ cells, but not Ngfr- cells, isolated
177 from denervated muscle (Suppl. Figure 4g). Finally, the Ngfr+ cells differed in phenotype and
178 morphology from the Ngfr- population, and unlike the Ngfr- cells, they did not show any myogenic
179 potential when cultured *in vitro* (Suppl. Figure 5a-b).
180 Interestingly, the presence of Ngfr+ cells was also observed in a mouse model of Spinal Cord
181 Injury (SCI) where the damage was induced by mechanical lesion of the spinal cord (Suppl. Figure
182 5c-d). Indeed, at 7 days post spinal lesion, the appearance of Ngfr+ cells was observed in TA muscle.
183 We found that in unperturbed muscles Plp1 positive cells are close to the neuron structure stained
184 for Neurofilament (NF-L) that is lost upon nerve injury. However, upon neve injury, Plp1+ /Ngfr+ cells
185 were found in a structure reminiscent of the nerve structure and close to bungarotoxin-positive NMJs

(Suppl. Figure 4a-c). Moreover, a decline in the number of the Ngfr+ cells and, more importantly, a decrease in the expression of neurotrophic factors was observed at 30 days after nerve injury, when the reinnervation process typically occurs (Suppl. Figure 6a-b).

Activated glial cells are known to respond to nerve injury and participate in nerve repair and axon guidance. To exclude the possibility that the presence of activated glial cells within the muscle was simply caused by co-isolation of adjacent tissues (i.e. nerves), we compared the gene expression profile of Ngfr+ cells isolated from nerves or muscles at 3 days after nerve injury (Figure 4a). Transcriptome analysis revealed significant differences between the two populations, which clearly formed two independent clusters with a large subset of differentially regulated genes (Figure 4a-c). Interestingly, among the genes differentially expressed by the two glial cells we found some genes more represented in muscle derived glial cells (i.e. Tnc, Gdnf), while others are more expressed in neuron derived cells (i.e. Shh) (Figure 4d). We focused on Tnc since its ablation is known to delay NMJ recovery in-vivo(27). Tnc protein unequivocally localized close to bungarotoxin (BTX)-positive NMJ upon denervation (Figure 4e-f and Suppl. Figure 6c). Finally, Tnc protein expression and localization close to the NMJ was observed in TA muscle at 7 days following spinal cord injury (Suppl. Figure 6d).

These results suggest an involvement of Tnc in the maintenance of NMJ following denervation.

Muscle resident glial cells activated by nerve injury adopt a defective neurotrophic phenotype in a mouse model for ALS.

The symptomatic stage of ALS is characterized by muscle denervation. Motoneuron degeneration leads to muscle atrophy and muscle weakness, ultimately accelerating disease progression (28). It is currently unclear whether the disease progression could be influenced by the neurotrophic activity of specialized cell types. We therefore set to determine whether an increased amount of muscle resident Plp1+/Ngfr+ glial cells could be observed at sequential stages of disease progression, using the $SOD1^{G93A}$ mouse model of ALS(29).

Indeed, Ngfr expression and Ngfr+ cells among Itga7+ cells increased with disease progression (Figure 5a-d). Ngfr expression displayed a striking increase in muscle derived from symptomatic SOD1^{G93A} at 90- and 140-days of postnatal life with a concomitant reduction of NF-L positive neurofilament in accordance with the progressive loss of muscle innervation (Figure 5b-d). Other factors such as Gdnf or Tenascin C also increased significantly in SOD1^{G93A} in the late stage of the disease (140d) compared to age-matched healthy animals (Figure 5d). Overall, these observations clearly identify muscle glial cells as potential players in the maintenance of nerve to muscle contact in the context of ALS. Interestingly, the magnitude of the induction of Tnc and Gdnf was clearly lower compared to acute denervation shown in Figure 1. This may account for the reduced reinnervation ability of SOD^{G93A} leading to muscle paralysis that marks the end-stage of the disease. In addition to the lower expression of Tnc compared to reversible nerve degeneration, we also observed a marked difference in Tnc localization in ALS muscle. Indeed, while in reversible denervation we observed a clear localization of Tnc protein close to the NMJ, in SOD^{G93A} muscle Tnc signal encircled muscle fibers without the NMJ associated pattern (Figure 5e-f). These data suggest a defect in the response of glial cells during disease progression.

To functionally validate the neurotrophic ability of Plp1+Ngfr+ muscle derived glial cells, we utilized an in-vitro transwell system (Figure 6a-c). Ngfr+ and Ngfr- cells were isolated from limb muscle of mice subjected to nerve injury or from symptomatic SOD^{G93A}, and co-cultured with the mouse motor neuron-like hybrid cell line (NSC-34), without direct contact through the use of specific trans-well inserts. Following 72h of co-culture in growth media, Ngfr+ cells from denervated muscle promoted NSC-34 neuronal differentiation when compared to control cells cultured under standard neuronal differentiation conditions, as documented by the increase in neurites length and the mean number of neurites per cell (Figure 6a-c). Conversely, this effect was not observed in NSC-34 co-cultured with Ngfr- cells. Interestingly, a lower ability to promote NSC-34 differentiation and neurite elongation was observed in cells co-cultured with Ngfr+ cells derived from SODG93A muscle (Figure 6a-c).

These data suggest that an impaired ability of muscle-resident glial cells to adopt a neurotrophic phenotype in response to nerve injury could contribute to progressive loss of NMJ in ALS muscles.

Next, given the localization of glial cells close to the NMJ, we explored the possibility that they may play a direct role in the promotion and maintenance of NMJ upon denervation. We tested this possibility by using a model of AChR clustering in cultured myotubes, previously described by Ngo and colleagues (30). As shown in Figure 6d-f and in Suppl. Figure7, conditioned media from muscle derived glial cells promote AChR clustering – as revealed by bungarotoxin staining – in differentiated C2C12 myotubes. As a positive control, 4h agrin (Agr) treatment was used. Interestingly, while after a 10' pulse of agrin followed by 4h of release the AChR clustering was reduced, as previously shown (30), replacement of conditioned media after agrin pulse led to a similar induction of AChR clustering compared to a full 4h agrin treatment. These observations support a direct role of muscle glial-released factors in the induction and maintenance of the muscle counterpart of the NMJ. Of note, we the formation of of AChR clustering was much attenuated when using conditioned media by glial cells isolated from the SOD^{G93A} muscle, further suggesting a functional impairment of muscle glial cell function during ALS progression.

DISCUSSION

scRNAseq-based analysis has been instrumental to unravel the heterogeneity of muscle-resident cells in unperturbed conditions, while highlighting their dynamic transitions through a continuum of functional cellular states and trajectories in response to homeostatic perturbations (22, 24, 31–37). These studies have used the typical experimental model of muscle regeneration, by physical injury, which leads to the sequential activation of multiple cell types, to reveal the identity of sub-populations endowed with specialized activities and their coordination in response to regeneration cues. In addition to MuSC activation, scRNAseq analyses has revealed a dramatic expansion and alteration of gene expression profiles in cells from the inflammatory infiltrate immediately after acute muscle injury (24, 34, 37). These cells account for the vast majority of the cell types present in muscles at early time points post injury and establish functional interactions with other cell types within the regenerative environment, including FAPs and MuSCs, to promote myofiber regeneration and injury resolution. As part of the regeneration process, the repair of injured nerve also occurs, although the cellular effectors of this process remain poorly understood. While earlier studies have suggested the potential contribution of MuSCs in the maintenance of NMJ

integrity and regeneration (9, 10), the precise identity of the cell types activated by nerve injury and their potential neurotrophic activity remain unknown.

Unlike muscle injury, nerve injury does not promote muscle regeneration, but leads to myofiber atrophy and muscle fibrosis (11, 38). These different outcomes are underpinned by differences in activated cell types. For instance, we have previously observed that muscle denervation leads to the selective activation of FAPs, which exhibit transcriptional profiles and biological activities different from FAPs activated in response to acute muscle injury (11, 31). Importantly, denervation does not trigger the massive infiltration of immune cells observed upon muscle injury (11). We argue that the lack of inflammatory infiltrate and the consequent reduction in the amount of inflammatory signals in the milieu of denervated muscles might account for the lack of activation of multiple cell types in denervated muscles (25). At the same time, the selective response of muscles to denervation might help to capture specific muscle-resident cells activated by nerve injury, without the potentially confounding co-existence of other activated cell types.

In this study, we describe a population of muscle-resident glial cells that are activated by nerve injury and might contribute to NMJ repair. These cells express Itga7 - a cell surface protein commonly used to prospectively isolate MuSCs (39). Indeed, both previously used FACS strategies and commercial kits could not distinguish the two populations due to the common antigen surface marker. A recent study identified a population of smooth muscle mesenchymal cells (SMMCs) within the FACS-isolated Itga7+ cells that is distinct from MuSCs (22). Interestingly, our results indicate that muscle-resident glial cells, while sharing Itga7 expression with MuSCs and SMMCs, exhibit a distinctive gene expression signature that is enriched in glial cell-specific genes. While some glial lineage-identity marker was constitutively expressed and could be used for their prospective isolation in unperturbed muscles (Plp1), a subset of neurotrophic genes was selectively expressed in these cells only in response to nerve injury. Among them, Ngfr was instrumental to further isolate the fraction of Itga7/Plp1 glial cells activated upon nerve injury (Figure 3). Ngfr is a receptor commonly associated with activated glial cells (40). Since Ngfr expression in Itga7-positive muscle glial cells is only observed upon their activation by nerve injury and coincides with the activation of the

298 neurogenic program, it is conceivable that Ngfr confers upon glial cells the competence to respond
299 to neurogenic signals.
300 Although nerve-associated glial-cells (otherwise defined as Schwann cells) are well known,
301 the biological properties of tissue-resident glial cells have only recently become the object of intense
302 investigation (41).
303 In the case of skeletal muscle, the specific function of peripheral glial cells and their regulation
304 in response to homeostatic perturbations, such as in ALS disease, are currently not well known (19,
305 42). Although several myelinating and non-myelinating cell types (Remak cells and terminal
306 Schwann cells) have been associated with neuron regeneration, a defined molecular signature able
307 to discriminate between subpopulations from different anatomical location and different functional
308 specialization has not been clearly identified. Indeed, the molecular features of terminal Schwann
309 cells remain mostly unknown, because their scarcity has so far impeded a comprehensive analysis
310 (43). Our data indicate that single cell RNA-seq based approaches may circumvent this issue due
311 to their potential to identify transcriptional signatures in a small number of cells within the pool of
312 cells analysed.
313 Our work identified a population of Itga7-expressing cells, distinct from MuSCs and SMMC,
314 that is selectively activated upon nerve injury and adopt a neurogenic gene expression profile and
315 functional neurotrophic properties. Interestingly, activated muscle resident glial cells localize in close
316 proximity to NMJs. While a comparative analysis using the scRNAseq profiles of Ngfr+ cells isolated
317 either from nerves or from muscles at 3 days post nerve injury revealed clear differences in gene
318 expression between these two populations, it is possible that they might represent two different
319 functional states of muscle-resident glial cells. Nevertheless, the differential expression of certain
320 genes, such as Tnc, Gdnf and Shh, suggests that muscle-resident glial cells adopt different
321 functional phenotypes in response to nerve injury.
322 The upregulation of Tnc in muscle-resident glial cells activated by nerve injury has not been
323 shown previously and highlights a fundamental difference between the skeletal muscle response to
324 nerve injury versus myotrauma. In this latter, Tnc is typically expressed by other types of resident-
325 muscle cells (e.g. FAPs) and accumulates within the ECM to regulate MuSC activity (23, 24, 34, 37).

Conversely, we show that in response to nerve injury, Tnc accumulates in close proximity to bungarotoxin (BTX)-positive NMJ. Thus, higher levels of Tnc in muscle-derived glial cells and its anatomical localization in proximity of NMJ are distinctive features of skeletal muscle response to NMJ injury. Considering that genetic ablation of Tnc causes delay in NMJ recovery in-vivo (27), we speculate that muscle glial-cell derived Tnc could contribute to NMJ repair following injury. This possibility is also supported by the finding that Tnc expression was reduced upon recovery of NMJ integrity (e.g. up to 30 days after lesion). It is possible that transient deposition of Tnc within the ECM at NMJ is an important event to promote NMJ repair and is part of a general program by which muscle glial cells commit to repair injured muscles. Consistently, we found that factors secreted by muscle glial cells could enhance AChR clustering in cultured myotubes.

Further studies will be necessary to investigate the actual contribution of muscle glial cells in the recovery of NMJ integrity in response to acute lesions or chronic degeneration, and whether these cells might be amenable to pharmacological manipulation to facilitate nerve repair. In this regard, pharmacological activation of the neurotrophic potential of muscle glial cells could be exploited in neurodegenerative disorders, such as ALS. A role for peripheral glial cells in ALS – and in particular pre-synaptic Schwann cells - has been recently suggested, although the precise mechanism of their involvement remains unknown (42, 44). We found a progressive increase of muscle resident glial cells in muscles of the ALS mouse model - $SOD1^{G93A}$ mice. However, activated muscle glial cells from symptomatic $SOD1^{G93A}$ mice exhibited reduced activation of neurotrophic genes, defective Tnc localization, impaired ability to promote neurite outgrowth/differentiation of a motoneuron cell line and to promote AChR clustering in cultured myotubes, as compared to glial cells activated in the context of acute reversible denervation. These data suggest that defective activity of muscle-glial cells could contribute to the pathogenesis of neurodegenerative diseases, such as ALS.

METHODS

Mouse Strains

Mouse strains used in this study were:

- C57BL/6J were provided by the Jackson Laboratory (Bar Harbor, USA).
- PAX7CreER/tdTomato$^{f/f}$ mice were provided by the SBP Animal Facility (La Jolla).
- Hemizygous transgenic mice carrying the mutant human SOD1^{G93A}(B6.Cg-Tg (SOD1*G93A)1Gur/J) gene were originally obtained from Jackson Laboratories (Bar Harbor, USA).
- CD1 were provided by Charles River Laboratories, Como, Italy.

All mice were maintained in a pathogen-free animal facility under standard 12h light/12h dark cycle at 21 °C with access to red house and to standard chow and water ad libitum. Three-month-old mice were used for ex-vivo experiments, except for the SOD1^{G93A} mice, as indicated in the Figure 5. For the denervation experiments, both male and female C57BL/6J and PAX7CreER/tdTomato$^{f/f}$ mice were used. Only female mice were used for the spinal cord injury experiment. As a mouse model of ALS male SOD1^{G93A} mice were used.

Cell Lines and Primary Cell Cultures

All cells were cultured in incubators at 37 °C and 5% CO_2. We used mouse MN-like NSC-34 cells (obtained from ATCC) which is a hybrid cell line produced by the fusion of MNs from the spinal cord embryos with N18TG2 neuroblastoma cells that exhibit properties of MNs after differentiation and maturation protocols(45). Thus, NSC-34 cells were grown in proliferation media [Dulbecco's Modified Eagle Medium: Nutrient Mixture *F-12* (*DMEM* / *F-12*, Sigma-Aldrich, D6421) supplemented with 10% of fetal bovine serum (FBS, Sigma, F4135) and 1% of Penicillin/Streptomycin (Gibco, 15070-063)]. Differentiation was induced by changing medium for DMEM-F12 plus 0.5% of FBS, 1% of non-essential amino acids (NEAA, Thermo Fisher Scientific, 11140050), 1% of Penicillin/Streptomycin.

Freshly isolated MuSCs and Ngfr+ cells were plated in 24-well plates in GM [DMEM [+Pyruvate] (Gibco, 41966-029), 20% FBS, 10% Hourse Serum, 1% Chick Embryo Extract (CEE)]. Myogenic differentiation was induced with DMEM and 2% horse serum for 2 or 3 days. NSC-34 and Ngfr+ cells were also used for co-culture experiments.

C2.12 (C2C12) myogenic cells were obtained from ATCC and cultured on 96-well plates in growth medium [DMEM [-Pyruvate] (Gibco, 61965-026), supplemented with 10% of FBS and 1% of Penicillin/Streptomycin]. Myogenic differentiation was induced by shifting the cells in differentiation medium (DMEM [-Pyruvate] complemented with 1% Penicillin/Streptomycin and 2% House Serum).

Acetylcholine receptor clustering assay

AChRs were considered to be a large AChR cluster when they were ≥ 25 μm in their longest dimension. C2C12 myotube were treated with 1 nM recombinat Rat Agrin (R&D System, 550-AG) for 4 hours or 10 minutes in differentiation medium (30). Different C2C12 myotube cultures were treated with conditioned media of muscle derived glial cells for 4h or after the 10' pulse of agrin. AChRs were labeled by the binding of Alexa Fluor 488 α-bungarotoxin (Invitrogen, B13422). Myotubes were incubated with the α-bungarotoxin diluted (1:300) in differentiation medium for 1 hours at 37°C in 5% CO_2. The number of AchR clusters per field in their longest dimension (≥ 25 μm) was measured by ImageJ.

Denervation

Unilateral hindlimb denervation was performed by clamping the left sciatic nerve under anesthesia by intraperitoneal injection of 40 mg/kg ketamine (Zoletil®, Virbac) and 10 mg/kg xylazine (Rampum, BAYER). Upon exposure of the sciatic nerve, the nerve was crushed for three times for 10 seconds. Alternative, for the bulk RNA-seq in Figure1a, nerve was cut with a scissor. The lesion was sutured after the operation.

Spinal cord injury

Three-month-old CD1 mice were used in SCI. To perform SCI, mice were deeply anaesthetized with a mixture 1:1 of Rompun (Bayer 20 mg ml^{-1}; 0.5 ml kg^{-1}) and Zoletil (100 mg ml^{-1}; 0.5 ml kg^{-1}), the back hairs were shaved, the skin was disinfected with betadine, and an incision was made to expose the spinal cord. Animals were mounted on a stereotaxic apparatus with spinal adaptors connected to a cortical PinPoint precision impactor device (Stoelting) and maintained at 37 °C throughout surgery. To induce a severe trauma the following parameters were set up: middle, round and flat tip (#4); velocity 3 m s^{-1}; depth 5 mm; dwell time 800 ms. The impact was applied at the thoracic level (vertebrae T10–T11). Analysis of the graphical impact parameters, operated by the PinPoint software, was used to identify potential outliers. Behavioural analyses were also used to corroborate differences in injury severity within groups. Slight lesions were excluded from the study based on these criteria.

Cell preparation and isolation by FACS

Tibialis anterior and gastrocnemius muscles, or nerves, of mice were subjected to enzymatic dissociation [in PBS with 2 mg/mL Collagenase A (Roche, 10 103 586 001), 2,4 U/mL Dispase I (Roche, 04 942 078 001), 10 ng/mL DNase (Sigma, 11 284 932 001), 0,4 mM $CaCl_2$ and 5mM $MgCl_2$] for 60 min at 37° C. The cell suspension was filtered through a 40-µm nylon filter and incubated with the following antibodies for 30 min: CD45 (Invitrogen, 48-0451-82), CD31 (Invitrogen, 48-0311-82), TER119 (Invitrogen, 48-5921-82), Sca1 (Invitrogen, 11-5981-82) and Itga7 (AbLab, R2F2), Ngfr (Miltenyi Biotec, 130-118-793).

Ngfr+ cells were isolated as TER119−/CD45−/CD31−/Itga7+/SCA-1−/Ngfr+ cells and Pax7-Tomato + as TER119−/CD45−/CD31−/Itga7+/SCA-1−/Tomato+ (Suppl.Figure1b).

In Suppl.Figure1a, satellite cell purification was performed by using SC Isolation Kit (Miltenyi Biotech, Bergisch Gladbach, Germany, 130-104-268).

Histology Immunofluorescence

For the histological analysis 8 µm muscle cryosection were analysed. Both cryosections and cultured cells were fixed in 4% PFA (Sigma, P6148) for 10 min and permeabilized with 100% acetone for 1 min at RT or with 0.1% Triton for 15 min at RT. Muscle sections and cultured cells were then blocked for 1h with a solution containing 4% BSA (Sigma, A7030-100G) in PBS. PAX7 staining was performed by an antigen retrieval protocol. The primary antibodies immunostaining was performed ON at 4°C and then the antibody binding specificity was revealed using secondary antibodies coupled to Alexa Fluor 488, 594, or 647 [Invitrogen, Goat anti-Mouse Alexa Flour 647 (1:400, A32728), Goat anti-Rabbit Alexa Flour 488 (1:400, A32731), Goat anti-Mouse Alexa Flour 488, (1:400, A32723)]. Acetylcholine receptors (AChRs) were revealed with fluorescently labeled Bungarotoxin (BTX) (1:500 Alexa 594, Invitrogen, B13423). Sections were incubated with DAPI (Thermo Fisher Scientific, D1306) in PBS for 5 minutes for nuclear staining, washed in PBS, and mounted with glycerol (3:1 in PBS).

The primary antibodies used for immunofluorescences are: rabbit anti-Plp1 (1:100, Cell Signaling, 28702S); mouse anti NFl (1:200, Santa Cruz Biotechnology, SC-20012); rat anti-Ngfr-PE (1:100, Miltenyi Biotec, 130-118-793); rabbit anti-Tnc (1:100, EMD Millipore Corp, AB19013); mouse anti-Caveolin-3 (1:1000, BD Transduction Laboratories, 610420); rabbit anti-Laminin (1:400, Sigma, L9393); anti BIII Tubulin mAb (1:500, PROMEGA, G712A); mouse anti-PAX7 (1:20, Developmental Studies Hybridoma Bank DSHB, Pax7); mouse anti-Myosin (1:10, Developmental Studies Hybridoma Bank DSHB, MF20); mouse α-Tubulin (1:200, Cell Signaling, #2144).

The transverse sections and cultured cells were visualized on a Zeiss confocal microscope then edited using the ImageJ® software. All histological analyses were performed in a blinded fashion. The figures reported are representative of all the examined fields.

EdU Proliferation Assay

Cell proliferation was measured by EdU incorporation. 20 mg per kg body weight EdU was administered intraperitoneally (i.p.) 12h before muscle harvest. Incorporation of EdU was revealed

using the “Click-iT™ EdU Cell Proliferation Kit for Imaging, Alexa Fluor™ 594 dye” (Thermo Fisher Scientific, C10354) following the manufacture protocol.

Co-culture conditions of Ngfr+ cells and NSC34

NSC-34 and Ngfr+ cells were cocultured by using inserts with 1µm porous membrane to avoid direct contact between populations. NSC-34 were grown independently from Ngfr+ in proliferation media for 48h in 24-well plates. After 24h, freshly sorted Ngfr+ cells were plated on the upper insert and transwell co-cultures were maintained for additional 72h in proliferation and differentiation media.

RNA analysis by quantitative PCR

RNA was extracted from cells using Qiagen RNeasy mini-kits (Qiagen, 74106) following the manufacturer’s protocol. Total RNA was quantified with a Nanodrop 8000 spectrophotometer (Thermo Scientific, Wilmington). First-strand cDNA was synthesized from total RNA using the Transcriptor First Strand cDNA Synthesis kit (Roche, N808-0234) following the manufacturer’s protocols. The generated cDNA was used as a template in real-time PCR reactions with 2x Fast Q-PCR Master Mix (SYBR, ROX) (SMOBIO, TQ1211) and was run on a Roche LC480 machine using three-step amplification and melt curve analysis. Quantitative real-time PCR reactions consisted of 2× SYBR Green Supermix, 0.25 μmol l^{-1} forward and reverse primers and 10 ng cDNA. Relative gene expression was normalized by dividing the specific expression value by the glyceraldehyde 3-phosphate dehydrogenase (Gapdh) expression value and calculated using the $2^{-\delta\Delta CT}$ method.
The following primer sets were used to identify transcripts:
Gapdh FW: CACCATCTTCCAGGAGCGAG, Gapdh RV: CCTTCTCCATGGTGGTGAAGAC,
Ngfr FW: TGCCTGGACAGTGTTACGTT, Ngfr RV: ACAGGGAGCGGACATACTCT,
Shh FW: CACCCCCAATTACAACCCCG, Shh RV: CTTGTCTTTGCACCTCTGAGTC,
Fgf5 FW: CTGTACTGCAGAGTGGGCAT, Fgf5 RV: AATTTGGCTTAACACACTGGC,
Runx2 FW: GCCTTCAAGGTTGTAGCCCT, Runx2 RV: GTTCTCATCATTCCCGGCCA,
Olig1 FW: CTCGCCCAGGTGTTTTGTTG, Olig1 RV: TAAGTCCGAACACCGATGGC,
Tnc FW: CTACCACAGAGGCCTTGCC, Tnc RV: AGCAGCTTCCCAGAATCCAC,

Pax7 FW: AGGACGACGAGGAAGGAGACA, Pax7 RV: TCATCCAGACGGTTCCCTTT

Vcam1 FW: GCACTCTACTGCGCATCTT, Vcam1 RV: CACCAGACTGTACGATCCT

Nrcam FW: ATGCACAGACATCAGTGGGG, Nrcam RV: GCTTGCCATTGCCTTCTTACC

Gdnf FW: TGGGTCTCCTGGATGGGATT, Gdnf RV: CGGCGGCACCTCGGAT

Rgs5 FW: CGCACTCATGCCTGGAAAG, Rgs5 RV: TGAAGCTGGCAAATCCATAGC

Myl9 FW: GCGCCGAGGACTTTTCTTCT, Myl9 RV: CCTCGTGGATGAAGCCTGAG

Plp1 FW: CCTAGCAAGACCTCTGCCAGTA, Plp1 RV: GGACAGAAGGTTGGAGCCACAA

Tamoxifen (Tmx) treatment and denervation

We used PAX7CreER/tdTomato$^{f/f}$ mice between the ages of 2 and 3 mouth for Tmx (Sigma, T5648) injections. Tmx (3 mg) suspended in corn oil was injected intraperitoneally (i.p.) each day for 5 d. After 7 d from the last injection, we performed the unilateral hindlimb denervation. Tissues were harvested after 3 d for FACS.

RNA-sequencing

MuSC were isolated from mice TA and GA muscle as described. RNA from MuSC was extracted using RNeasy Mini kit (Qiagen) following the manufacturer's protocol. RNA was shipped to the sequencing IGA of Udine. The libraries for sequencing were prepared using NuGEN Ovation System V2 RNA-Seq. For each biological sample two independent experiments were carried out for the isolation of RNA. All duplicates are pool of three different mice, sorted at different times.

RNA-sequencing data processing

For sequencing alignment we used the mouse reference genome assembly GRCm38/mm10 (http://ftp.ensembl.org/pub/release-76/fasta/ mus_musculus/dna/), and for transcriptome annotation we used version 85 of the GRCm38 (http://ftp.ensembl.org/pub/release85/gtf/mus_musculus/Mus_musculus. GRCm38.85.gtf.gz). We used the FASTQC package (v0.11.3) to assess the quality of sequenced libraries. All passed quality control. Reads were mapped to the reference genome using TopHat2 v.2.1.1. The quality control of

519 the reads distribution along transcripts was performed using infer_experiment.py from RSeQC
520 package v2.6.3. All samples had a uniform distribution of reads along transcripts. The sequenced
521 read counts per annotated gene were derived with the use of htseq-count script distributed with
522 HTSeq v0.5.4p5. We used the R library package DESeq2 v.1.12.4 for measuring differential gene
523 expression between two different cell conditions, considering the two RNA–seq experiments as
524 biological replicates. We picked genes with adjusted P value < 0.001. Gene ontology analysis was
525 performed using David 6.8 (https://david.ncifcrf.gov/). In details Biological Process was predicted on
526 genes differentially expressed with p adjusted<0.01 with the following setting: threshold counts=2,
527 threshold EASE=0.1. The most significant 12 functional annotation was illustrated in the figure.
528
529 **Single-cell RNA-sequencing**
530 Single-cell RNA-sequencing was performed at IGA facility of Udine - Italy
531 (https://igatechnology.com/). Methanol fixed cells were rehydrated following 10X Genomics
532 recommendation. In order to remove visible debris, an additional washing in Wash-Resuspension
533 buffer was introduced. Cell concentration was determined using the Countess II FL Automated Cell
534 Counter (Thermo Fisher Scientific, Waltham, MA). Trypan Blue staining of the methanol fixed cells
535 showed that 100% of the cells were dead, indicating that all cells were effectively fixed and
536 permeabilized.
537 Chromium controller and Chromium NextGEM Single Cell 3' Reagents Kit v3.1 (10X Genomics,
538 Pleasanton, CA) have been used for partitioning cells into Gel Beads-in-emulsion (GEMs), where all
539 generated cDNA share a common 10x barcode. Libraries were generated from the cDNA following
540 manufacturer's instruction and checked with both Qubit 2.0 Fluorometer (Invitrogen, Carlsbad, CA)
541 and Agilent Bioanalyzer DNA assay (Agilent technologies, Santa Clara, CA). Libraries were then
542 prepared for sequencing and sequenced on NovaSeq6000 (Illumina, San Diego, CA) with the
543 following run parameters: Read 1=28 cycles, i7 index=8 cycles, Read 2=91 cycles.
544
545
546

Single-cell RNA-sequencing data processing.

The raw sequencing data were processed by Cell Ranger v 3.1.0 (10X Genomics) with mouse transcriptome reference mm10 to generate gene-cell expression matrices. Further data analysis was carried out in R version 3.6.0 using Seurat version 3.1.1(46). The two datasets were set up as independent Seurat objects. ‘‘Cells’’ that fit any of the following criteria were filtered out: < 200 or > 4,500 expressed genes, or > 10% UMIs mapped to mitochondria. Dataset normalization and identification of variable features were performed using the NormalizeData() function and the FindVariableFeatures() with following parameters (selection.method = "vst", nfeatures = 4000). Integration anchors were computed using the first 20 dimensions, using all the genes present in both datasets as features to integrate. Finally, we obtained 3949 cells that passed quality control, with an average of 1,460 genes expressed per cell. For downstream integrated analyses, top 30 components were used for PCA, UMAP and cluster identification (using a resolution of 0.4). Further, we manually assigned cell population identity based on cell-type-specific markers and merged those clusters that displayed similar canonical markers. After clustering and cell population identification, the most highly differentially expressed genes, or putative cluster markers, were identified by a likelihood-ratio test using the FindAllMarkers() function with the following parameters(only.pos = TRUE, min.pct =0.5, min.diff.pct=0.25, logfc.threshold = 0.25). Genes differentially expressed in CTR vs DEN where identified using the FindMarkers() function and subsequently filtered using the following criteria (pct.1>0.45 or pct.2>0.45; p_val_adj<0.01; avg_logFC< (-0.58) or avg_logFC>0.58). Dataset Integration with previously published scRNAseqs (Giordani and De Micheli) has been performed in Seurat with FindIntegrationAnchors() and IntegrateData() functions using the first 20 dimensions. From the De Micheli dataset, only the uninjured datapoint ("D0") has been used for comparison. Both datasets were downloaded from the GEO website.

Figure Design

Graphical abstract, Figure 1d, Figure 4a, Figure 6b and Figure 6e were created with BioRender (https://biorender.com/)

Statistics

Data are presented as mean with SD. Statistical analysis was performed using Graph Pad Prism 8.0 software (Pad Software). Normality was tested by Shapiro-Wilk test. Unpaired, two-tailed Student's t test was used to compare the means of two parametric groups, while Mann-Whitney test for two non-parametric groups. One-way ANOVA with Tukey's post-test was used for comparison among the different parametric data sets. Significance was defined as $P < 0.05$ (*), $P < 0.01$ (**), and $P < 0.001$ (***).

The number of biological replicates for each experiment is indicated in the figure legends. RNAseq data was performed in 2 independent samples derived from different animals. Statistical method was Deseq2. Right-tailed Fisher's exact test and one-sided Fisher's exact test was used for IPA analyses. For scRNA-seq, biological sample replicates came also from separate mice. Histological and Immunofluorescence images are representative of at least 3 different experiment/animals. For cell culture studies, biological replicates from separate culture wells.

Data and code availability

a7int+ mouse bulk RNA-sequencing data, Mouse Single Cells RNA-sequencing data and Ngfr+ Mouse bulk RNA-sequencing data are available at the SRA repository (Accession numbers: PRJNA623246, PRJNA626530 and PRJNA649152).

STUDY APPROVAL

All experiments in this study were performed in accordance with protocols approved by the Italian Ministry of Health, National Institute of Health (IIS), and Santa Lucia Foundation (Rome) and by the Sanford Burnham Prebys Medical Discovery Institute Animal Care and Use Committee. The study is compliant with all relevant ethical regulations regarding animal research and in the respect of the principles of the 3Rs (Replacement, Reduction and Refinement).

AUTHOR CONTRIBUTIONS

Designing Research Studies, D.P., PL.P. and LM.; conducting experiments, D.P. and L.M.; investigation, D.P., L.M., M.D., L.G., C.D., S.M.; resources, L.M., A.S., M.A., M.B., C.V., PL.P.; analyzing data, D.P., L.G., S.A. and L.M.; writing—original draft preparation, L.M.; writing—review and editing, L.M., L.G., PL.P., B.LO., C.V., and M.B.; supervision, L.M., PL.P.; project administration, funding acquisition, L.M. and PL.P.

ACKNOWLEDGMENTS

This work was supported by the Italian Ministry of Health (grant no. GR-2013- 02356592) and Roche per la Ricerca 2019 to L.M.; R01AR076247-01 NIH/NIAMS to PLP; Muscular Dystrophy Association (MDA) grant# 418870, National Institute of Health (NIH) R01AR064873 to A.S.; The Dutch Duchenne Parent Project NL (DPP NL) to B.L.O.; The Parent Project Italy (PP, Italy) and University of Rome to M.B.

Finally, we thank the Italian Ministry of Health (Ricerca Corrente) that have supported the research performed in this work.

The authors thank E. Aleo at the Institute of Applied Genomics in Udine, Italy, for RNA–seq library preparation and sequencing, L. Battistini for flow cytometry related discussions and advice, the authors also thank P. Longone, A. Spalloni, A. Renzini and M. Loreti for the help provided.

620 **REFERENCES**

621 1. Farup J, Madaro L, Puri PL, Mikkelsen UR. Interactions between muscle stem cells,
622 mesenchymal-derived cells and immune cells in muscle homeostasis, regeneration and disease.
623 *Cell Death Dis.* 2015;6(7):e1830–e1830.
624 2. Bentzinger CF, Wang YX, Dumont NA, Rudnicki MA. Cellular dynamics in the muscle satellite
625 cell niche. *EMBO Rep.* 2013;14(12):1062–1072.
626 3. Mauro A. Satellite cell of skeletal muscle fibers. *J Biophys Biochem Cytol* 1961;9:493–495.
627 4. Wosczyna MN, Rando TA. A Muscle Stem Cell Support Group: Coordinated Cellular Responses
628 in Muscle Regeneration. *Dev Cell* 2018;46(2):135–143.
629 5. Feige P, Brun CE, Ritso M, Rudnicki MA. Orienting Muscle Stem Cells for Regeneration in
630 Homeostasis, Aging, and Disease. *Cell Stem Cell* 2018;23(5):653–664.
631 6. Baghdadi MB, Tajbakhsh S. Regulation and phylogeny of skeletal muscle regeneration. *Dev.*
632 *Biol.* 2018;433(2):200–209.
633 7. García-Prat L, Sousa-Victor P, Muñoz-Cánoves P. Proteostatic and Metabolic Control of
634 Stemness. *Cell Stem Cell* 2017;20(5):593–608.
635 8. Brack AS, Rando TA. Tissue-specific stem cells: lessons from the skeletal muscle satellite cell..
636 *Cell Stem Cell* 2012;10(5):504–14.
637 9. Liu W, Wei-LaPierre L, Klose A, Dirksen RT, Chakkalakal J V. Inducible depletion of adult
638 skeletal muscle stem cells impairs the regeneration of neuromuscular junctions. *Elife* 2015;4.
639 doi:10.7554/eLife.09221
640 10. Liu W et al. Loss of adult skeletal muscle stem cells drives age-related neuromuscular junction
641 degeneration. *Elife* 2017;6. doi:10.7554/eLife.26464
642 11. Madaro L et al. Denervation-activated STAT3-IL-6 signalling in fibro-adipogenic progenitors
643 promotes myofibres atrophy and fibrosis. *Nat Cell Biol* 2018;20(8):917–927.
644 12. Sakaguchi S et al. Implication of anti-inflammatory macrophages in regenerative moto-
645 neuritogenesis: Promotion of myoblast migration and neural chemorepellent semaphorin 3A
646 expression in injured muscle. *Int. J. Biochem. Cell Biol.* 2014;54:272–285.
647 13. Tatsumi R et al. Possible implication of satellite cells in regenerative motoneuritogenesis: HGF

upregulates neural chemorepellent Sema3A during myogenic differentiation. *Am. J. Physiol. - Cell Physiol.* 2009;297(2). doi:10.1152/ajpcell.00161.2009

14. Pradat PF et al. Abnormalities of satellite cells function in amyotrophic lateral sclerosis. *Amyotroph Lateral Scler* 2011;12(4):264–271.

15. Scaramozza A et al. Skeletal muscle satellite cells in amyotrophic lateral sclerosis. *Ultrastruct Pathol* 2014;38(5):295–302.

16. Sandri M. Protein breakdown in muscle wasting: role of autophagy-lysosome and ubiquitin-proteasome. *Int J Biochem Cell Biol* 2013;45(10):2121–2129.

17. Glass DJ. Signalling pathways that mediate skeletal muscle hypertrophy and atrophy. *Nat. Cell Biol.* 2003;5(2):87–90.

18. Braun T, Gautel M. Transcriptional mechanisms regulating skeletal muscle differentiation, growth and homeostasis. *Nat. Rev. Mol. Cell Biol.* 2011;12(6):349–361.

19. Li L, Xiong W-C, Mei L. Neuromuscular Junction Formation, Aging, and Disorders. *Annu. Rev. Physiol.* 2018;80(1):159–188.

20. Tiwari N et al. Stage-Specific Transcription Factors Drive Astrogliogenesis by Remodeling Gene Regulatory Landscapes.. *Cell Stem Cell* 2018;23(4):557-571.e8.

21. Magill CK et al. Reinnervation of the tibialis anterior following sciatic nerve crush injury: a confocal microscopic study in transgenic mice. *Exp Neurol* 2007;207(1):64–74.

22. Giordani L et al. High-Dimensional Single-Cell Cartography Reveals Novel Skeletal Muscle-Resident Cell Populations. *Mol. Cell* 2019;74(3):609-621.e6.

23. Tierney MT et al. Autonomous Extracellular Matrix Remodeling Controls a Progressive Adaptation in Muscle Stem Cell Regenerative Capacity during Development. *Cell Rep.* 2016;14(8):1940–1952.

24. De Micheli AJ et al. Single-Cell Analysis of the Muscle Stem Cell Hierarchy Identifies Heterotypic Communication Signals Involved in Skeletal Muscle Regeneration. *Cell Rep.* 2020;30(10):3583-3595.e5.

25. Nicoletti C et al. scRNA-seq-based analysis of skeletal muscle response to denervation reveals selective activation of muscle-resident glial cells and fibroblasts. *bioRxiv* 2020;2020.12.29.424762.

676 26. Hicks MR et al. ERBB3 and NGFR mark a distinct skeletal muscle progenitor cell in human
677 development and hPSCs. *Nat Cell Biol* 2018;20(1):46–57.
678 27. Cifuentes-Diaz C et al. Abnormal reinnervation of skeletal muscle in a tenascin-C-deficient
679 mouse. *J. Neurosci. Res.* 2002;67(1):93–99.
680 28. Kiernan MC et al. Amyotrophic lateral sclerosis. In: *The Lancet*. Elsevier; 2011:942–955
681 29. Tu PH et al. Transgenic mice carrying a human mutant superoxide dismutase transgene
682 develop neuronal cytoskeletal pathology resembling human amyotrophic lateral sclerosis lesions.
683 *Proc. Natl. Acad. Sci. U. S. A.* 1996;93(7):3155–3160.
684 30. Ngo ST, Cole RN, Sunn N, Phillips WD, Noakes PG. Neuregulin-1 potentiates agrin-induced
685 acetylcholine: Receptor clustering through muscle-specific kinase: Phosphorylation. *J. Cell Sci.*
686 2012;125(6):1531–1543.
687 31. Malecova B et al. Dynamics of cellular states of fibro-adipogenic progenitors during
688 myogenesis and muscular dystrophy. *Nat Commun* 2018;9(1):3670.
689 32. Der Vartanian A et al. PAX3 Confers Functional Heterogeneity in Skeletal Muscle Stem Cell
690 Responses to Environmental Stress. *Cell Stem Cell* 2019;24(6):958-973.e9.
691 33. Dell'Orso S et al. Single cell analysis of adult mouse skeletal muscle stem cells in homeostatic
692 and regenerative conditions. *Development* 2019;146(12):dev174177.
693 34. Oprescu SN, Yue F, Qiu J, Brito LF, Kuang S. Temporal Dynamics and Heterogeneity of Cell
694 Populations during Skeletal Muscle Regeneration. *iScience* 2020;23(4).
695 doi:10.1016/j.isci.2020.100993
696 35. Schaum N et al. Single-cell transcriptomics of 20 mouse organs creates a Tabula Muris
697 [Internet]. *Nature* 2018;562(7727):367–372.
698 36. Scott RW, Arostegui M, Schweitzer R, Rossi FMV, Underhill TM. Hic1 Defines Quiescent
699 Mesenchymal Progenitor Subpopulations with Distinct Functions and Fates in Skeletal Muscle
700 Regeneration. *Cell Stem Cell* 2019;25(6):797-813.e9.
701 37. Pawlikowski B et al. A cellular atlas of skeletal muscle regeneration and aging. *bioRxiv*
702 2019;635805.
703 38. Rebolledo DL et al. Denervation-induced skeletal muscle fibrosis is mediated by CTGF/CCN2

independently of TGF-β. *Matrix Biol.* [published online ahead of print: February 2019]; doi:10.1016/J.MATBIO.2019.01.002

39. Pasut A, Jones AE, Rudnicki MA. Isolation and culture of individual myofibers and their satellite cells from adult skeletal muscle. *J. Vis. Exp.* 2013;(73):e50074.

40. Jessen KR, Mirsky R. The origin and development of glial cells in peripheral nerves. *Nat. Rev. Neurosci.* 2005;6(9):671–682.

41. Carr MJ et al. Mesenchymal Precursor Cells in Adult Nerves Contribute to Mammalian Tissue Repair and Regeneration. *Cell Stem Cell* 2019;24(2):240-256.e9.

42. Lasiene J, Yamanaka K. Glial cells in amyotrophic lateral sclerosis. *Neurol. Res. Int.* 2011;2011. doi:10.1155/2011/718987

43. Alvarez-Suarez P, Gawor M, Prószyński TJ. Perisynaptic schwann cells - The multitasking cells at the developing neuromuscular junctions. *Semin. Cell Dev. Biol.* 2020;104:31–38.

44. Arbour D, Vande Velde C, Robitaille R. New perspectives on amyotrophic lateral sclerosis: the role of glial cells at the neuromuscular junction. *J. Physiol.* 2017;595(3):647–661.

45. Cashman NR et al. Neuroblastoma × spinal cord (NSC) hybrid cell lines resemble developing motor neurons. *Dev. Dyn.* 1992;194(3):209–221.

46. Stuart T et al. Comprehensive Integration of Single-Cell Data. *Cell* 2019;177(7):1888-1902.e21.

Proietti et al. Figure 1

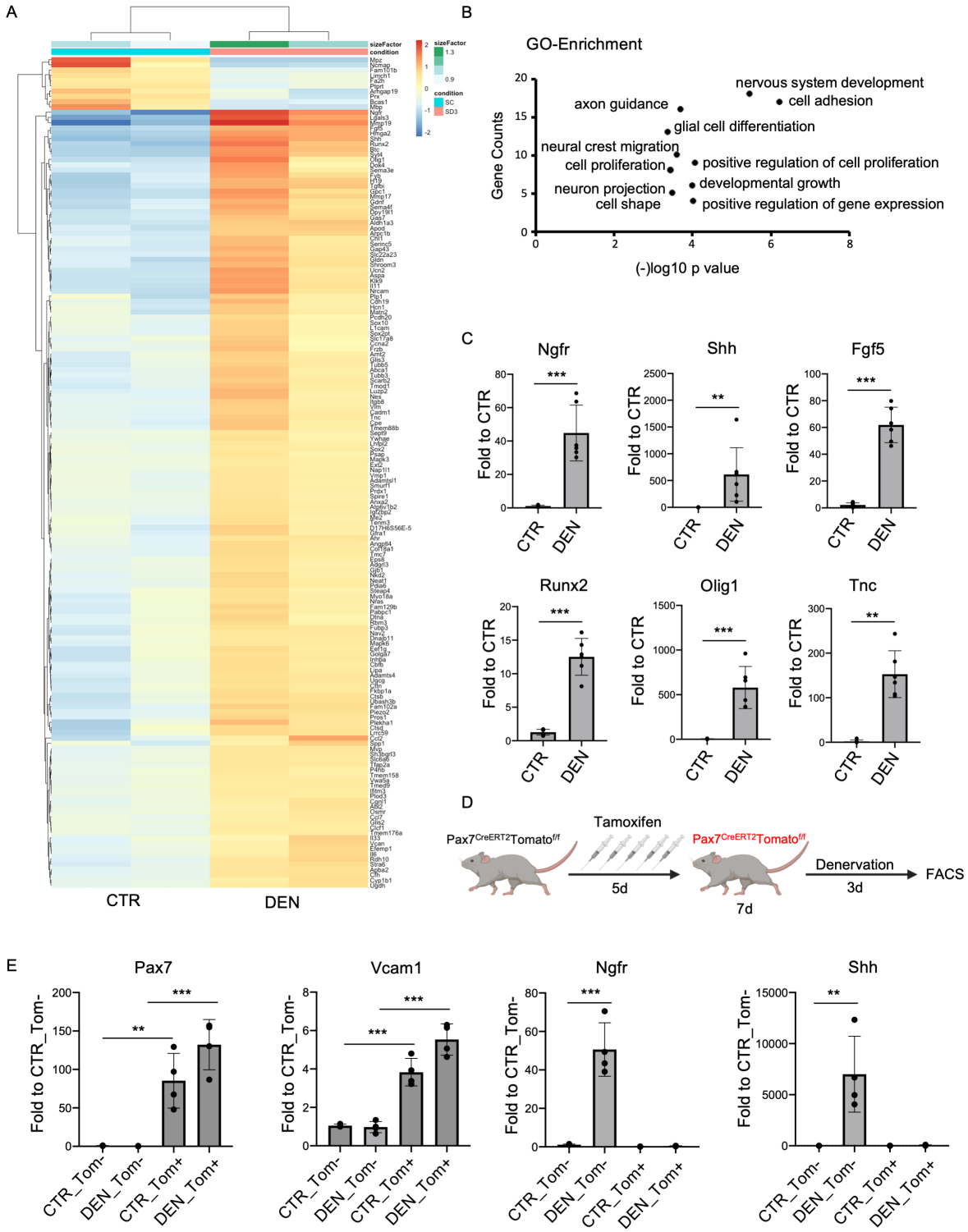

723

724

Figure 1. Activation of a neurotrophic signaling pathway in the Itga7+Sca1-Ln- myogenic cell fraction.

A) Heatmap representation of genes significantly deregulated - p adj<0.001 - in Itga7+Sca1-Ln- freshly isolated cells derived from denervated (cut) muscle at 3-days post nerve lesion (n=2). **B)** GO-Enrichment in Biological Function (BF) of genes significantly deregulated - p adj<0.001 - in Itga7+Sca1-Ln- cells derived from at 3 days denervated muscle. **C)** qPCR analysis for the expression of Ngfr, Shh, Fgf5, Runx2, Olig1 and Tnc in freshly isolated Itga7+Sca1-Ln- cells derived from control and 3 days reversible denervated (crush) muscle. Gapdh was used as housekeeping gene ($n \geq 5$, Values represent mean ± s.d. **P < 0.01 and ***P < 0.001; by student t-test (Ngfr, Fgf5, Olig1, Runx2, Shh) or by Mann-Whitney test (Tnc)). **D)** Working model of tamoxifen induced in-vivo treatment. **E)** qPCR analysis for the expression of Pax7, Vcam1, Ngfr and Shh in freshly isolated Tomato+ and Tomato- cells derived from control and 3 days denervated muscle of tamoxifen treated PAX7.Cre_tdTomato mice. Gapdh was used as housekeeping gene (n=4, Values represent mean ± s.d. **P < 0.01 and ***P < 0.001; by One Way Anova Tukey's Multiple Comparisons test).

Proietti et al. Figure 2

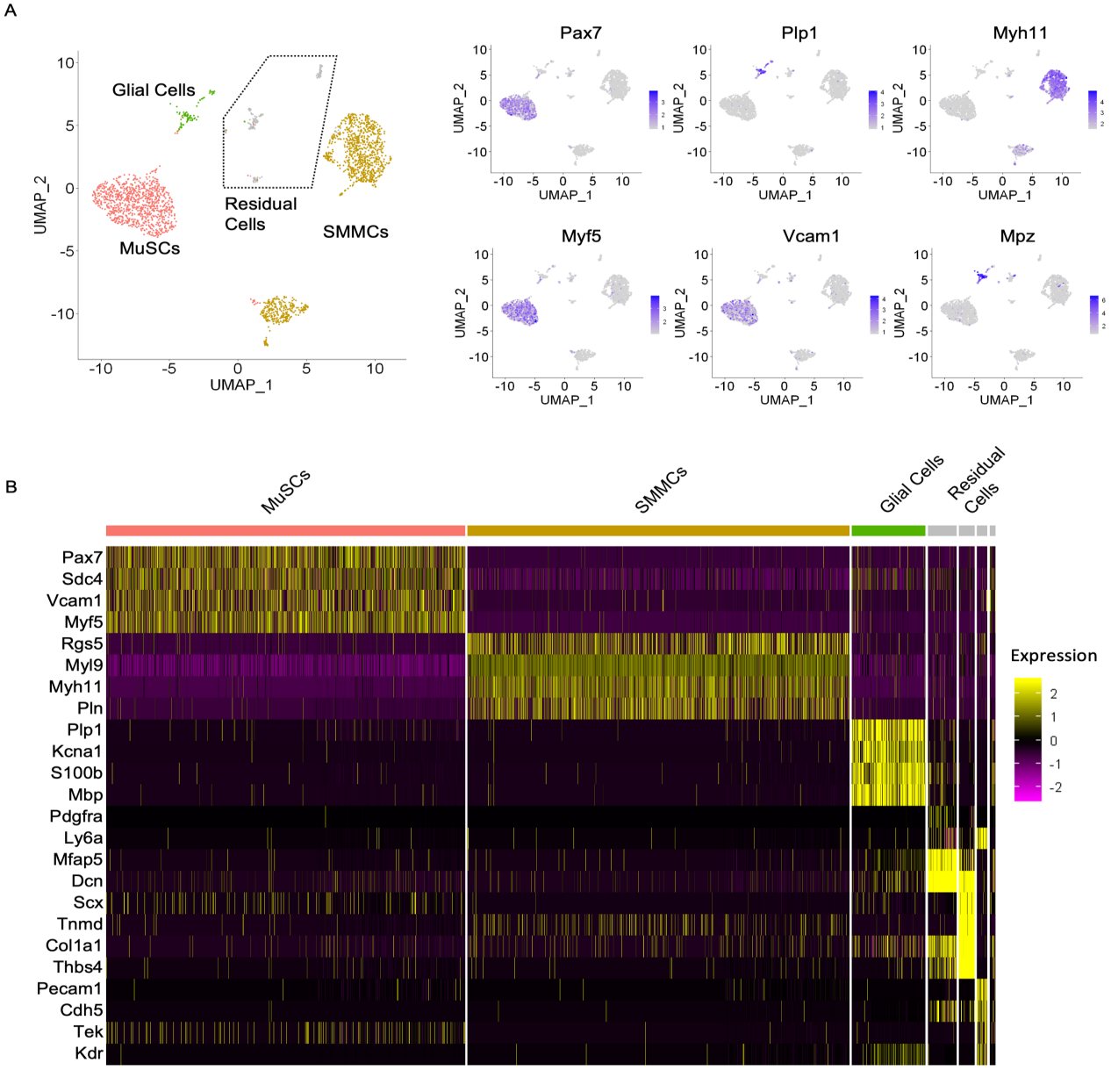

740
741

Figure 2. Itga7+ cell heterogeneity revealed by scRNA-seq analysis.

A) Distribution of Pax7, Plp1, Myh11, Myf5, Vcam1 and Mpz transcripts in Uniform Manifold Approximation and Projection (UMAP)-derived clusters of single cells (Single Cells RNA-seq) of Itga7+Sca1-Ln- isolated cells from control muscle. **B)** RNA expression heatmap for the given cell populations (column) and genes (row), sorted by clusters. The canonical markers used to identify each cluster are plotted (or the most variable genes per cluster in cases where markers were not already present in the literature).

Proietti et al. Figure 3

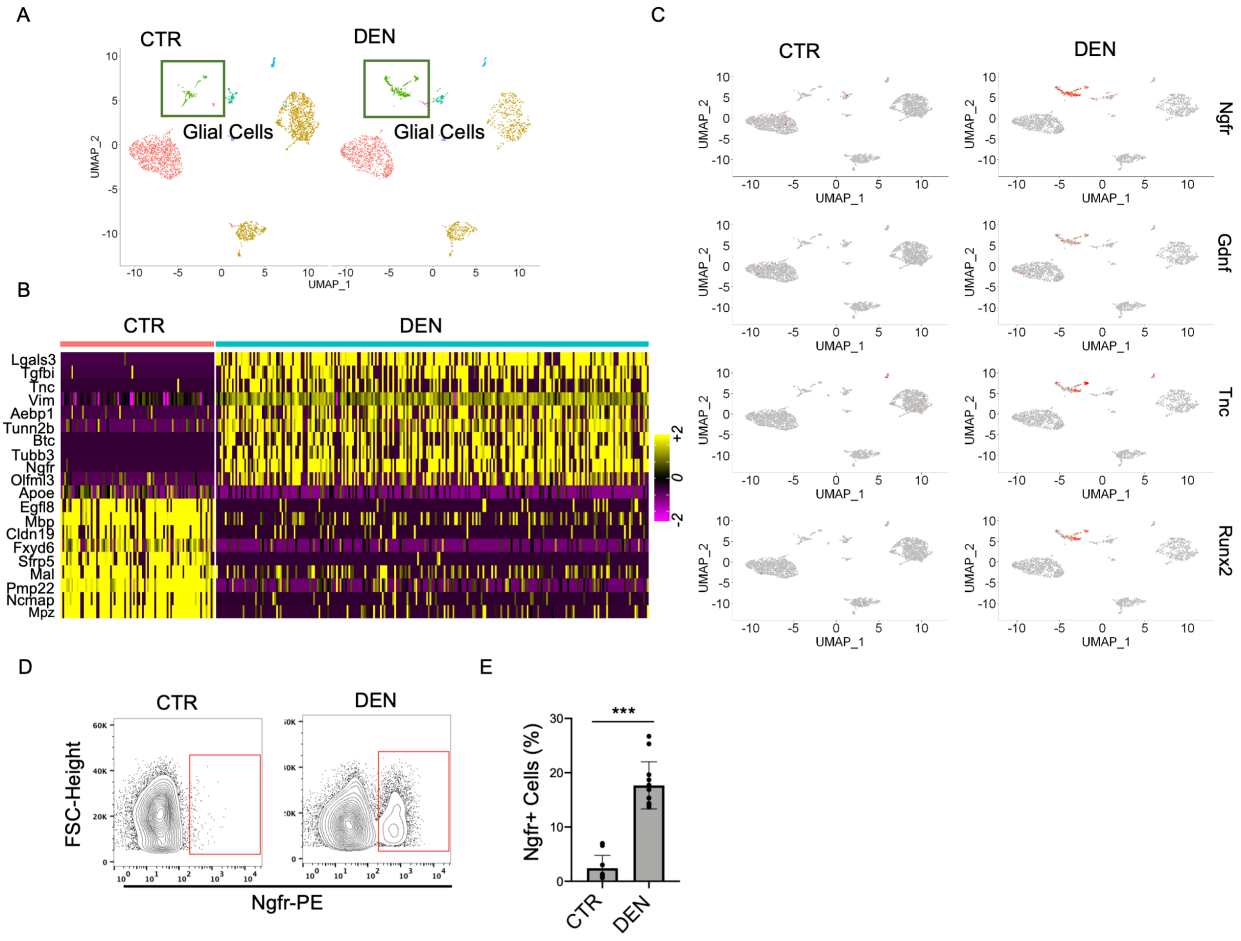

750

751

Figure 3. Activation of a neurotrophic signalling pathway in muscle glial cells upon denervation.

A) Distribution in Uniform Manifold Approximation and Projection (UMAP)-derived clusters of single cells (Single Cells RNA-seq) of Itga7+Sca1-Ln- isolated cells from control (CTR-left) and 3-days denervated muscle (DEN-right). **B)** RNA expression heatmap for Plp1 cell populations isolated from control and denervated muscle (row) and genes (column), sorted by clusters. **C)** Distribution of Ngfr, Gdnf, Tnc and Runx2 transcripts in Uniform Manifold Approximation and Projection (UMAP)-derived clusters of single cells (Single Cells RNA-seq) of Itga7+Sca1-Ln- isolated cells from control (left) and denervated (right) muscle. **D)** Representative cytofluorimetric plot of Ngfr+ - gated within the Itga7+Sca1-Ln- population - cells in control (left) and denervated (right) muscle. **E)** Quantification of Ngfr+ cells was shown in the graphs as a percentage of Itga7+Sca1-Ln- population (n=8 CTR, n=10 DEN, Values represent mean ± s.d. ***P < 0.001; by Mann-Whitney test).

Proietti et al. Figure 4

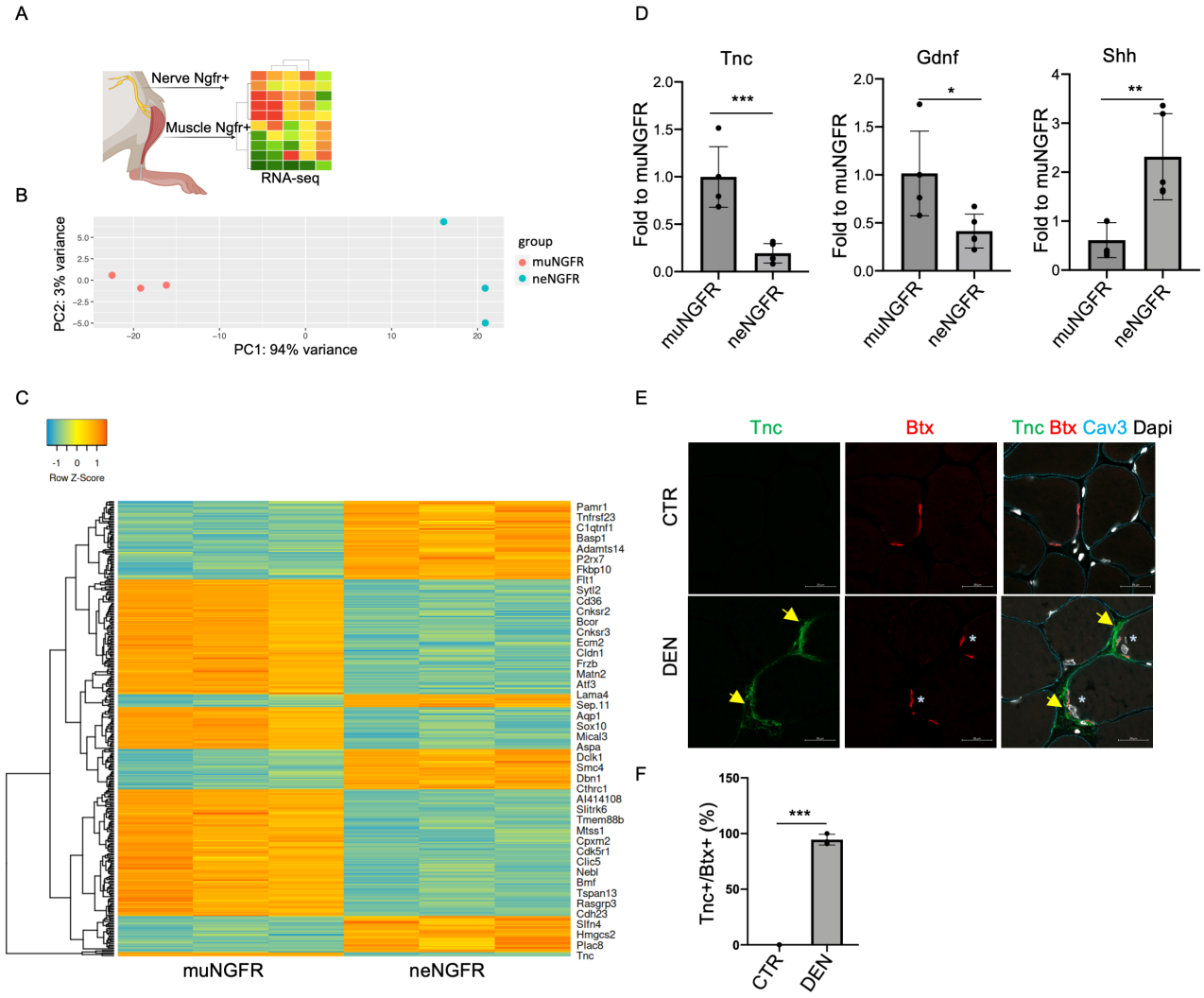

Figure 4. A specific transcriptional signature distinguishes glial cells in muscle from those residing in the nerve

A) Experimental setting for RNA-sequencing analysis of Ngfr+ cells derived from denervated muscle and nerve at 3-days post nerve lesion. **B)** Sample distance - represented as Principal component analysis (PCA) - of transcriptome of Ngfr+ cells derived from denervated muscle and nerve at 3-days post nerve lesion (n=3). **C)** Heatmap representation of genes significantly deregulated - p adj<0.001 – in freshly isolated Ngfr+ cells derived from denervated muscle and nerve at 3-days post nerve lesion (n=3). **D)** qPCR analysis for the expression of Tnc, Gdnf and Shh in freshly isolated Ngfr+ cells derived from denervated muscle (muNGFR) and nerve (neNGFR) at 3-days post nerve lesion (n=4, Values represent mean ± s.d. .*P < 0.05, **P < 0.01 and ***P < 0.001; by student t-test (Tnc, Gdnf) or by Mann-Whitney (Shh)). **E)** Representative immunofluorescence analysis of TA muscle cryosection derived from control and denervated muscle, stained for Tnc (green), Bungarotoxin (Btx, red) and Caveolin-3 (Cav3, Cyan). Arrows highlight Tnc and asterisk highlight Btx. Nuclei were counterstained with dapi. Scale bar = 20μm. **F)** Quantification Bungarotoxin (Btx) and Tnc co-localization in control and denervated muscle (n=3, Values represent mean ± s.d. ***P < 0.001; by student t-test)

Proietti et al. Figure 5

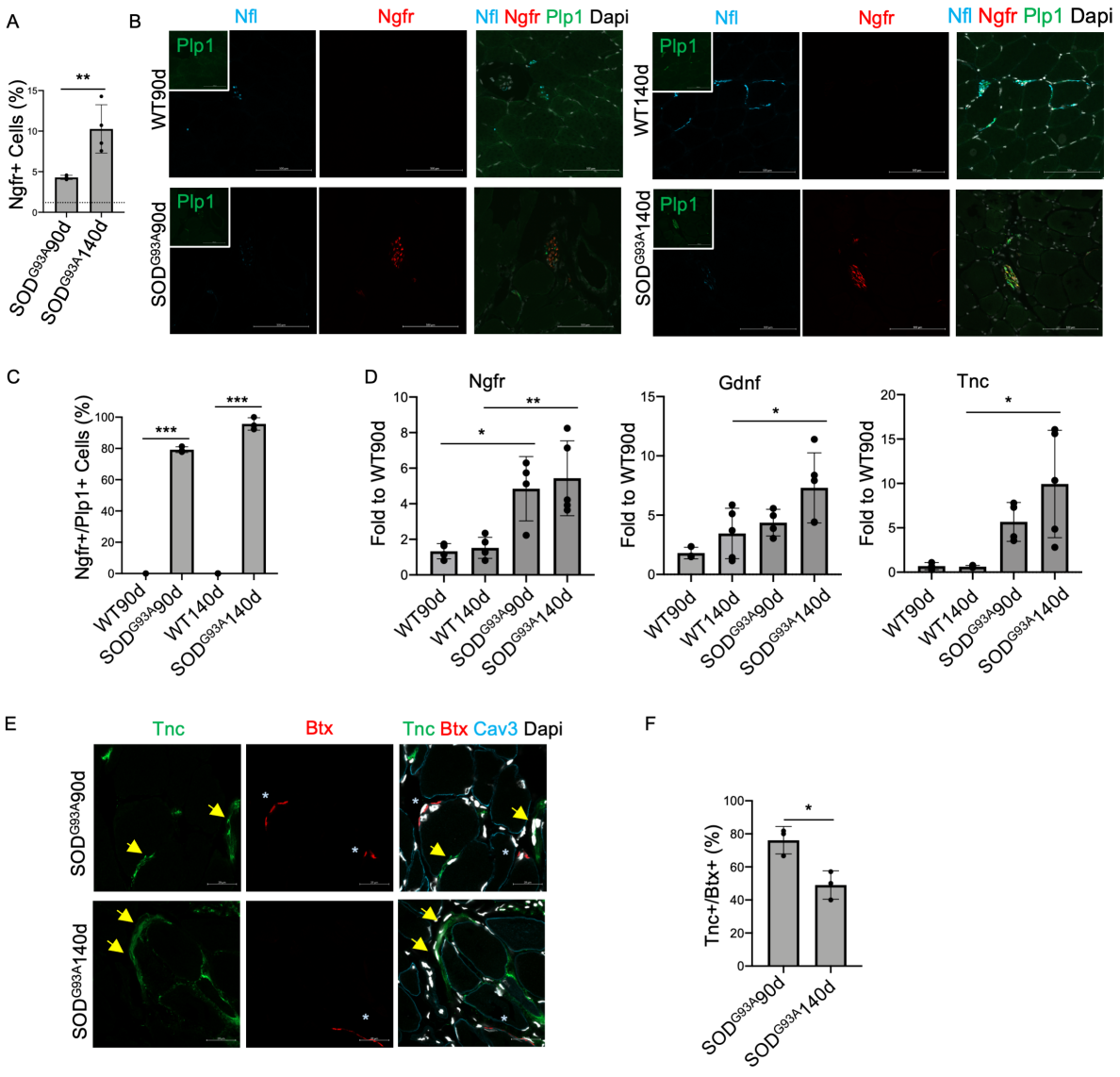

785

786

Figure 5. Muscle resident glial cell activation in a mouse model of ALS.

A) Ngfr+ cell cytofluorimetric quantification was shown in the graphs as a percentage of Itga7+Sca1-Ln- population, in 90- and 140-days old SOD^{G93A} mice muscle (n=4, Values represent mean ± s.d. **P < 0.01; by One Way Anova Tukey's Multiple Comparisons test). Dotted line highlight percentage in WT mice muscle. **B)** Representative immunofluorescence analysis of TA muscle cryosection derived from 90- and 140-days old SOD^{G93A} and WT mice stained for Neurofilament-L (Nfl, Cyan), Ngfr (red) and Plp1 (green). Nuclei were counterstained with dapi. Scale bar = 100μm. **C)** Quantification graph of Ngfr+/Plp1+ cells in 90- and 140-days old WT and SOD^{G93A} mice muscle (n=3, Values represent mean ± s.d. ***P < 0.001; by One Way Anova Tukey's Multiple Comparisons test) **D)** qPCR analysis for the expression of Ngfr, Gdnf and Tnc in freshly isolated Itga7+Sca1-Ln- cells derived from WT and SOD^{G93A} muscle at 90- and 140-days of post-natal life. Gapdh was used as housekeeping gene (n=4, Values represent mean ± s.d. *P < 0.05 and **P < 0.01; by One Way Anova Tukey's Multiple Comparisons test). **E)** Representative immunofluorescence analysis of TA muscle cryosection derived from 90- and 140-days old SOD^{G93A} and WT mice stained for Tnc (green), Bungarotoxin (Btx, red) and Caveolin-3 (Cav3, Cyan). Arrows highlight Tnc and asterisk highlight Btx. Nuclei were counterstained with dapi. Scale bar = 20μm. **F)** Quantification of Bungarotoxin (Btx) and Tnc co-localization in 90- and 140-days old SOD^{G93A} mice muscle (n=3, Values represent mean ± s.d. *P < 0.05; by student t-test)

Proietti et al. Figure 6

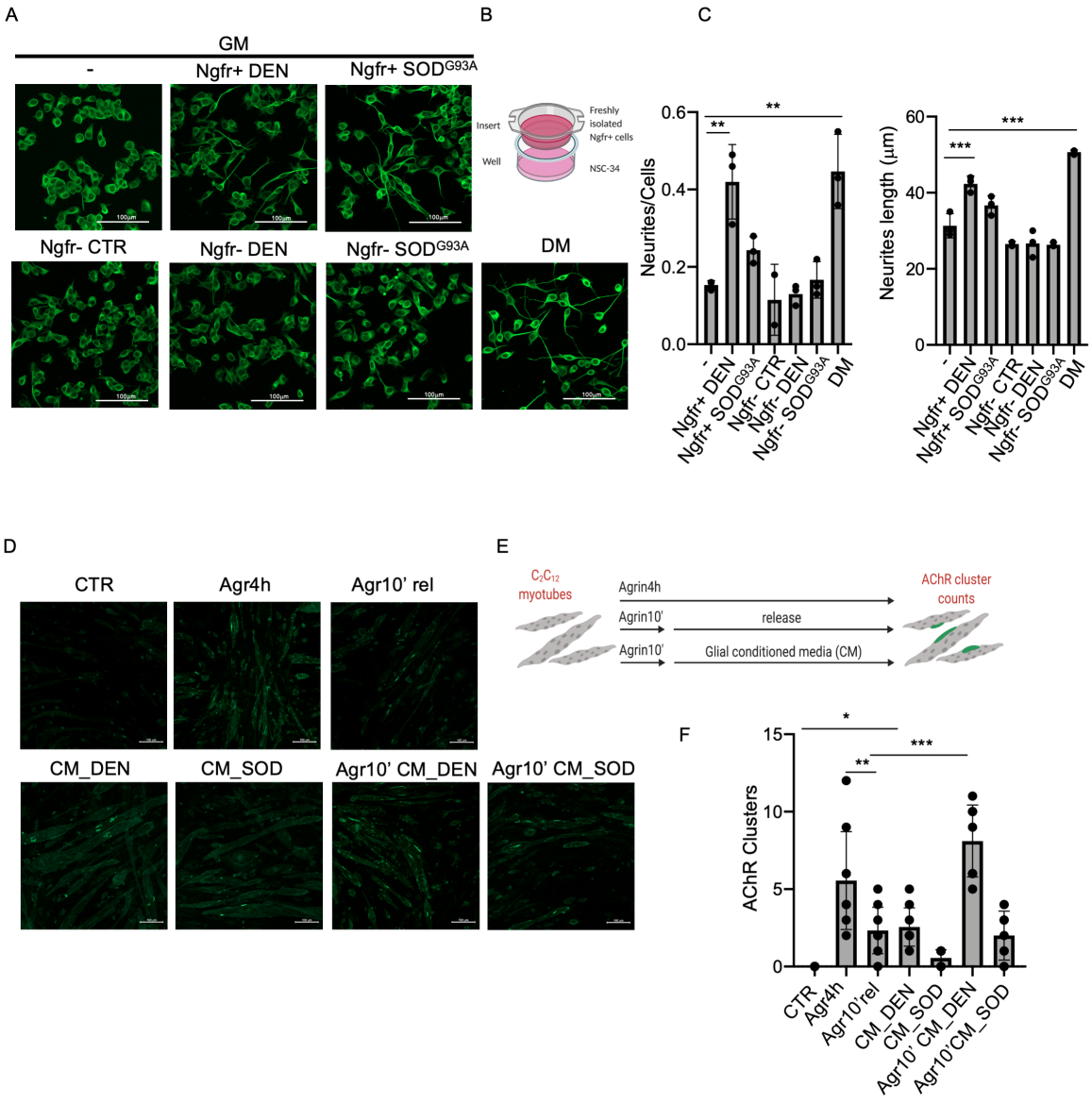

806

807

Figure 6. Muscle resident glial cells promote neurite outgrowth and AChR clustering.

A) Representative immunofluorescence analysis of NSC-34 cells in growth media cultured either alone (-) or in co-culture with Ngfr+ or with Ngfr- cells, both from denervated muscle and SOD^{G93A} muscle at 90-days of post-natal life, and of NSC-34 cells cultured in neurogenic differentiation media (DM), stained for beta-3-Tubulin (green). Scale bar = 100μm. **B)** Schematic representation of in-vitro co-culture system. **C)** Quantification of neurites number per cell and length of NSC-34 cultured in the indicated conditions (n=3, Values represent mean ± s.d. **P < 0.01 and, **P < 0.01; by One Way Anova Tukey's Multiple Comparisons test). **D)** Representative immunofluorescence analysis of C2C12 myotubes treated or not with Agrin or conditioned media from glial cells as indicated and stained with Bungarotoxin (Btx, green). Scale bar = 100μm. **E)** Schematic representation of the experimental setting. **F)** Quantification of AChR clustering (≥ 25 μm) (n=5, Values represent mean ± s.d.. *P < 0.05, **P < 0.01, ***P < 0.001; by One Way Anova Tukey's Multiple Comparisons test).